# Optimizing Interface Conductivity in Electronics

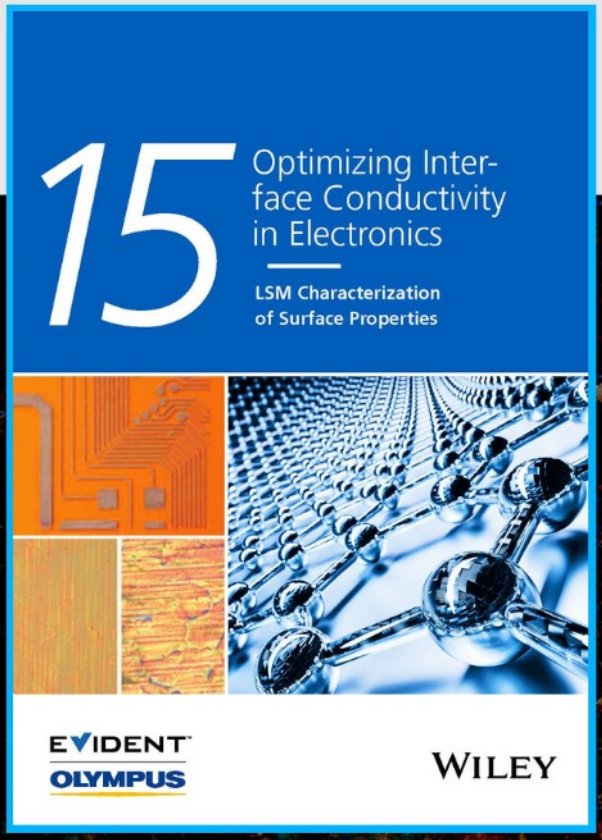


**The latest eBook from Advanced Optical Metrology. Download for free.**

Surface roughness is a key parameter for judging the performance of a given material's surface quality for its electronic application. A powerful tool to measure surface roughness is 3D laser scanning confocal microscopy (LSM), which will allow you to assess roughness and compare production and finishing methods, and improve these methods based on mathematical models.

Focus on creating high-conductivity electronic devices with minimal power loss using laser scanning microscopy is an effective tool to discern a variety of roughness parameters.

EVIDENT
OLYMPUS

WILEY

ADVANCED FUNCTIONAL MATERIALS
www.afm-journal.de



# Exciton Formation Dynamics and Band-Like Free Charge-Carrier Transport in 2D Metal Halide Perovskite Semiconductors

*Silvia G. Motti, Manuel Kober-Czerny, Marcello Righetto, Philippe Holzhey, Joel Smith, Hans Kraus, Henry J. Snaith, Michael B. Johnston, and Laura M. Herz**

**Metal halide perovskite (MHP) semiconductors have driven a revolution in optoelectronic technologies over the last decade, in particular for high-efficiency photovoltaic applications. Low-dimensional MHPs presenting electronic confinement have promising additional prospects in light emission and quantum technologies. However, the optimisation of such applications requires a comprehensive understanding of the nature of charge carriers and their transport mechanisms. This study employs a combination of ultrafast optical and terahertz spectroscopy to investigate phonon energies, charge-carrier mobilities, and exciton formation in 2D $(PEA)_2PbI_4$ and $(BA)_2PbI_4$ (where PEA is phenylethylammonium and BA is butylammonium). Temperature-dependent measurements of free charge-carrier mobilities reveal band transport in these strongly confined semiconductors, with surprisingly high in-plane mobilities. Enhanced charge-phonon coupling is shown to reduce charge-carrier mobilities in $(BA)_2PbI_4$ with respect to $(PEA)_2PbI_4$. Exciton and free charge-carrier dynamics are disentangled by simultaneous monitoring of transient absorption and THz photoconductivity. A sustained free charge-carrier population is observed, surpassing the Saha equation predictions even at low temperature. These findings provide new insights into the temperature-dependent interplay of exciton and free-carrier populations in 2D MHPs. Furthermore, such sustained free charge-carrier population and high mobilities demonstrate the potential of these semiconductors for applications such as solar cells, transistors, and electrically driven light sources.**

## 1. Introduction

Metal halide perovskite (MHP) semiconductors have given rise to exciting developments in optoelectronic applications over the past decade. Among their main achievements to date are solar cell devices reaching record efficiencies above 25%.[1] MHPs form a versatile family of semiconductors with tunable bandgaps and high photoluminescence quantum efficiencies,[2] making them also promising materials for light emitting diodes[3–6] and lasers.[7–11] In addition, the exploitation of low-dimensional MHPs presenting electronic confinement has demonstrated great potential for developing quantum emitters.[12–16] One strategy for producing quantum confinement in MHP semiconductors is the incorporation of large organic cations during the fabrication process, which can lead to the self-assembly of 2D quantum wells.[17,18] 2D Ruddlesden-Popper perovskites can be fabricated with a wide variety of organic cations, with the general formula $A_2B_{n-1}M_nX_{3n+1}$, where M is a metal, X is I, Br, or Cl, A is a large cation that acts as a spacer, and B is a cation small enough to fit into the

S. G. Motti, M. Kober-Czerny, M. Righetto, P. Holzhey, J. Smith, H. Kraus, H. J. Snaith, M. B. Johnston, L. M. Herz
Clarendon Laboratory, Department of Physics
University of Oxford
Parks Road OX1 3PU, Oxford, UK
E-mail: laura.herz@physics.ox.ac.uk

The ORCID identification number(s) for the author(s) of this article can be found under https://doi.org/10.1002/adfm.202300363.



**DOI: 10.1002/adfm.202300363**

S. G. Motti
School of Physics and Astronomy, Faculty of Engineering and Physical Sciences
University of Southampton
University Road SO17 1BJ, Southampton, UK

L. M. Herz
TUM Institute for Advanced Study
Technische Universität München
Lichtenbergstr. 2a, 85748 Garching bei München, Germany

lead halide cage of a conventional 3D perovskite lattice. The parameter $n$ determines the relative fraction of small and large cations and hence the degree of confinement. While strong confinement is achieved with $n = 1$, mixed compositions with larger $n$ can be tailored to create energy cascades.[3,4,19] Furthermore, the properties of the metal-halide semiconductor layers can be modulated by choice of organic spacers.[20–22] Layered 2D MHPs have also been successfully employed in photovoltaic devices, mainly with larger $n$ (i.e., low degree of confinement), improving the environmental stability and reducing non-radiative recombination losses.[23–26] While the versatility of 2D perovskites offers a multitude of exciting application prospects, some stipulated aspects, such as higher exciton binding energies, higher charge-carrier recombination rates, and lower mobilities compared with 3D bulk MHPs[27,28] could be potentially detrimental. Therefore, a complete assessment of such effects on free charge-carrier formation and transport is urgently required. In this context, the interplay of bound and free electron-hole pairs in these semiconductors is still an open question, despite being a key aspect for all optoelectronic applications.

In this work, we investigate the interplay of exciton and free charge-carrier populations, the charge-carrier mobilities, and the charge-phonon couplings in 2D lead halide perovskites employing ultrafast temperature-dependent optical and terahertz spectroscopy. We study highly oriented, phase-pure thin films of 2D perovskite in the Ruddlesden–Popper (RP) configuration, formed by individual layers of lead iodide octahedra ($n = 1$) separated by different organic cations, either butylammonium (BA) or phenylethylammonium (PEA). We reveal band transport with high charge-carrier mobilities in the lead-iodide semiconductor plane that depend on the choice of the organic spacer. Furthermore, we record the exciton formation dynamics on the picosecond timescale by terahertz and optical transmission transients. Our findings reveal a sustained, long-lived free-charge population that violates the predictions of the Saha equation, the most commonly used model for calculating ratios of free charge-carrier to exciton populations in these semiconductors. Overall, our work demonstrates highly efficient transport properties driven by a significant population of mobile free charge carriers. Our findings demonstrate the outstanding potential for optoelectronic applications of 2D MHP semiconductors, in particular for photovoltaics and electrically-driven light emitters that strongly rely on efficient charge transport.

## 2. Results and Discussion

### 2.1. Optical and Vibrational Properties

Thin films of 2D RP perovskite $(PEA)_2PbI_4$ (PEPI) and $(BA)_2PbI_4$ (BAPI) have been deposited on quartz substrates (see methods for details).[29] Grazing-incidence wide-angle X-ray scattering (GIWAXS) shows the films to be highly oriented with the lead-iodide semiconducting planes parallel to the substrate (see Section S1, Supporting Information). These data also show the presence of a single phase associated with $n = 1$ octahedra, as would be expected in the absence of smaller A-cations. **Figure 1** shows the absorption and photoluminescence

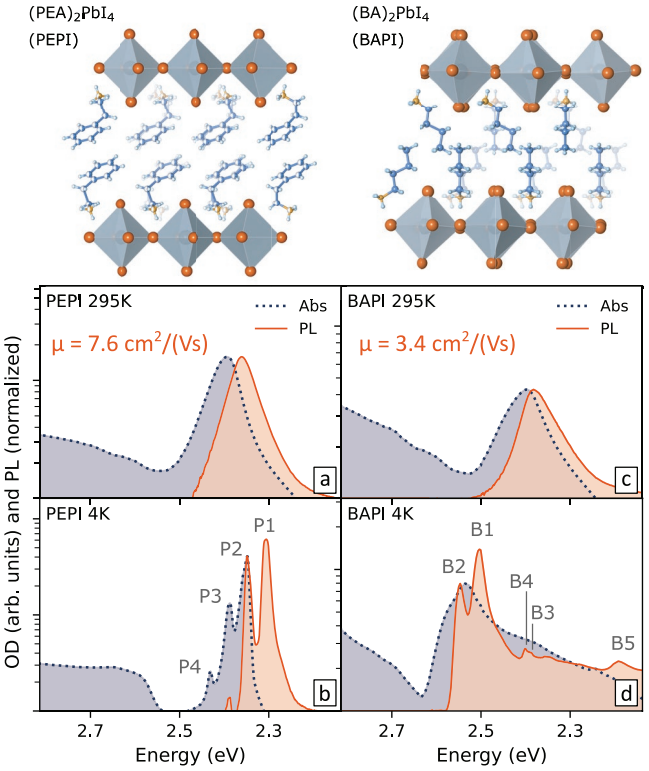


**Figure 1.** Absorption and PL spectra of PEPI ($(PEA)_2PbI_4$) at a) room temperature (295K) and b) 4K; and BAPI ($(BA)_2PbI_4$) at c) room temperature (295K) and d) 4K.

(PL) spectra of PEPI and BAPI thin films at different temperatures. Both materials exhibit strong excitonic absorption peaks at the band-edge that can be resolved into multiple lines at lower temperatures.[30,31] Four exciton lines in PEPI are similarly separated by ≈38 meV and have been previously assigned either to a vibronic progression of the exciton[32,33] or distinct exciton-polarons.[34–36] The changes in the absorption and PL of PEPI and BAPI with increasing temperature (**Figure 2**a,b) can be described by a combination of an increase in the bandgap, an increase in relative Stokes shift,[37] and a gradual shift of the dominant emission line from P1/B1 to P2/B2 following a temperature-activated behavior.[38] An abrupt shift marks a phase transition in BAPI around 270K.[39–41] We note that a residual phase mixture is still present in BAPI even at 4K, leading to additional features observed in the absorption and PL spectra associated with the high-temperature phase, which are marked in Figure 1d as B4 and B3. Another peak at lower energies (B5, at ≈2.2 eV) can be observed in the PL spectrum at low temperature and has been previously assigned to defect states or self-trapped excitons.[40]

Based on the Elliott formula,[42–44] and the direct observation of the band-edge onset, we determine exciton binding energies ($E_B$) of approximately ≈210 meV for PEPI and ≈250 meV for BAPI (see Section S3, Supporting Information, for details). These values are not substantially affected by temperature[45] and agree with previous reports in the literature.[28,45–47] The larger values of $E_B$ observed in BAPI with respect to PEPI can be explained by the stronger dielectric mismatch between the organic spacer and the lead iodide layers and, consequently,

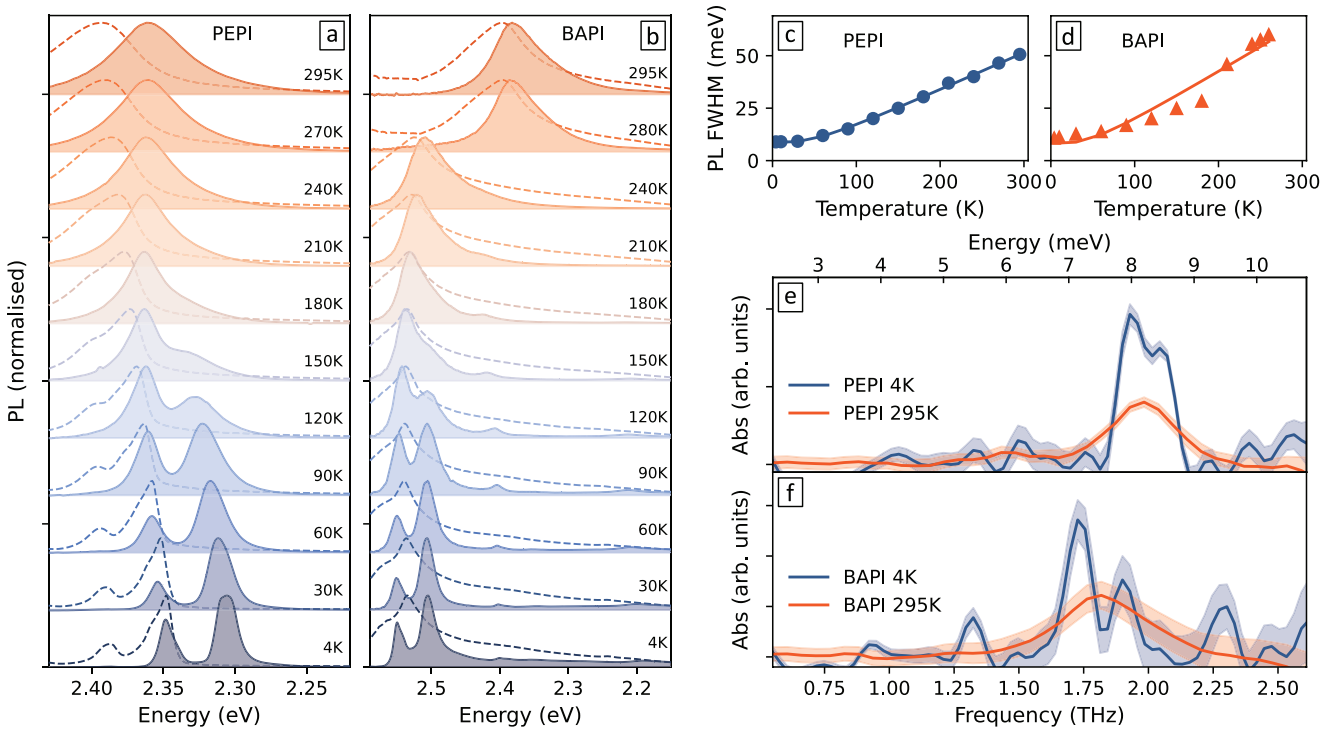


**Figure 2.** Temperature dependence of the PL of a) PEPI ($(PEA)_2PbI_4$) and b) BAPI ($(BA)_2PbI_4$), dashed lines show the absorption spectra. FWHM of the main band-edge PL peak of c) PEPI and d) BAPI (B2 and P2, respectively) as a function of temperature are displayed as dots. The solid line shows the fit to a combination of inhomogeneous broadening and phonon coupling. e,f) THz absorption spectra at 4K (blue) and 295K (red) for (e) PEPI and f) BAPI.

stronger dielectric confinement of the exciton.[20] However, we note that the presence of multiple exciton lines, broadening, and disorder typically complicate the analysis of $E_B$ in these materials.

The temperature dependence of the PL lineshape also offers interesting insights into the charge-phonon coupling mechanisms at play.[31,46,48,49] The full width at half-maximum (FWHM) of the dominant band-edge PL peak in PEPI (P2) and BAPI (B2) is shown as a function of temperature in Figure 2c,d. In lead halide perovskite semiconductors, the Fröhlich interaction with longitudinal optical (LO) phonons has been reported to be the dominant contribution to homogeneous PL broadening.[50] Our THz experiment is capable of measuring the absorption spectra of transverse optical (TO) phonon modes, from which we derive the corresponding LO phonon frequencies using the Lyddane–Sachs–Teller (LST) relation between the static and high-frequency values of the dielectric function[51] (see Section S5, Supporting Information, for details). From the frequency of the pronounced TO phonon mode observed in the THz absorption spectra of PEPI and BAPI and the LST relation, we obtain $E_{LO}$ = 11.8 meV for PEPI and $E_{LO}$ = 11.3 meV for BAPI . We employ these values as fixed parameters in fits to the FWHM of the PL based on a Bose-Einstein term to capture the temperature dependence[50] (see Section S6, Supporting Information, for details) and obtain coupling strengths of $\gamma_{LO}$ = 25 meV for PEPI and $\gamma_{LO}$ = 32 meV for BAPI , indicating stronger coupling of charge carriers to optical phonon modes of the polar lead iodide lattice for BAPI . We note, however, that such analysis of FWHM can be somewhat affected by inhomogeneous broadening, the presence of multiple peaks in these 2D RP semiconductors, [52] and the presence of residual phase mixtures.

### 2.2. Charge Transport

Such analysis of the temperature-dependent emission line broadening provides intriguing initial insight into charge transport properties in the 2D perovskites, as electron-phonon coupling is one of the key factors regulating charge-carrier mobilities in these semiconductors.[53] To directly investigate the charge-carrier mobilities in PEPI and BAPI, we employ optical-pump terahertz-probe (OPTP) photoconductivity spectroscopy. The OPTP experiment provides a non-contact measure of the sheet photoconductivity $\Delta S$ induced by the incidence of pulsed photoexcitation.[27,54,55] The effective electron-hole sum mobility $\mu_{eff} = \phi\mu$ , where $\phi$ is the photon-to-free-charge branching ratio, is calculated from the $\Delta S$ amplitude immediately after pulsed 3.1 eV photoexcitation (see Section S2, Supporting Information, for details). In the films studied, the semiconductor planes are highly oriented parallel to the substrate (see GIWAXS in Section S1, Supporting Information). Therefore, the electric field vector of the incoming THz radiation probes the in-plane mobility within the semiconductor layers. We obtain mobility values of $\mu_{eff}$ = 7.6 $cm^2/(Vs)$ for PEPI and $\mu_{eff}$ = 3.4 $cm^2/(Vs)$ for BAPI at room temperature (295 K). The lower mobility of BAPI agrees well with our observations of increased electron-phonon coupling strength and lower LO phonon frequencies in

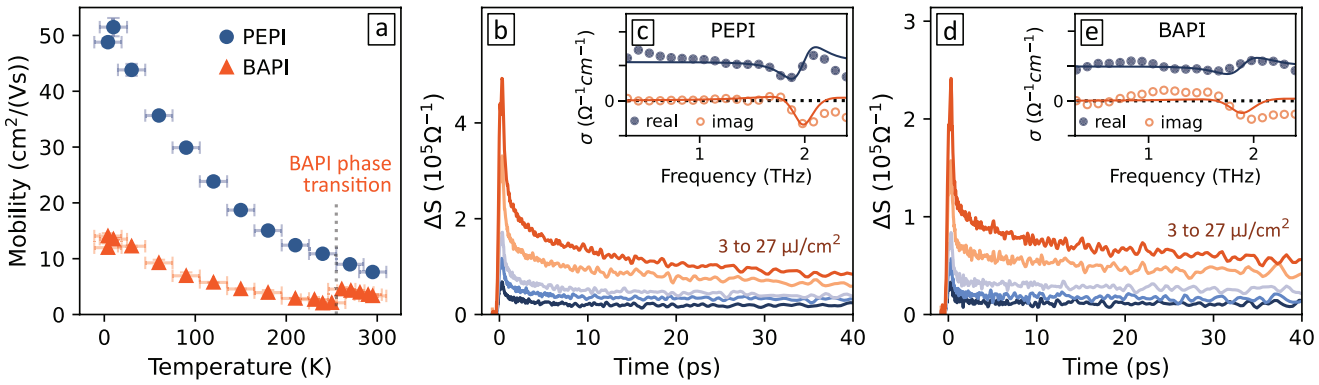


**Figure 3.** a) Charge-carrier mobilities, calculated from the OPTP sheet photoconductivity ΔS signal immediately after photoexcitation with a 3.1 eV laser pulse, as a function of temperature for PEPI (blue) and BAPI (red). OPTP photoconductivity transients obtained with various intensities of 3.1 eV photoexcitation of b) PEPI and d) BAPI at room temperature (295 K). Complex OPTP photoconductivity spectra of c) PEPI and e) BAPI obtained at room temperature at ≈ 2 ps time delay following 3.1 eV photoexcitation. The solid lines show the fitted spectra as a combination of Drude conductivity with a photoinduced phonon shift.

BAPI with respect to PEPI. These observations also agree with previous reports of increased lattice softness in BAPI,[56] which will induce a softening of optical modes and increase in Fröhlich coupling at a given temperature.[57] Such significant variations of lattice dynamics and charge-carrier mobilities observed between PEPI and BAPI are particularly interesting considering their similar dimensionality, bandgap, and inorganic framework composition. Our findings thus demonstrate the substantial impact of the organic spacer in these Ruddlesden-Popper perovskites, which is in remarkable contrast to their 3D counterparts with $ABX_3$ stoichiometry, where choice of organic cations on the A site plays a very minor role in dictating the optical phonon frequencies and intrinsic charge-carrier mobilities.[53,57]

We proceed by analysing the temperature dependence of charge-carrier mobilities (**Figure 3**a) in order to examine the mechanism of transport in these semiconductors. PEPI and BAPI show a clear trend of increasing mobilities with decreasing temperatures. This is clear evidence of band transport, for which electron-phonon coupling is reduced at lower temperatures,[50] similar to the trends observed in 3D perovskites.[58] This interesting observation of band transport demonstrates an absence of small polaron formation that would manifest itself as thermally-activated hopping transport and decreasing mobilities at low temperature.[59] We also note an abrupt change in the mobility values of BAPI at the phase transition temperature as a response to the relaxation of the octahedral tilting. Although previous reports have suggested that the enhanced anharmonic lattice fluctuations would contribute to reduced mobilities in the room temperature phase of BAPI,[41] our experimental findings clearly demonstrate higher mobility above the phase transition. This interesting observation is in agreement with theoretical predictions of lower charge-carrier mass in the room-temperature phase compared to the low-temperature phase in BAPI, as reported by Ziegler et al.[60] The band-transport trend shown in Figure 3a has also been observed in BAPI by Gèlvez–Rueda et al. based on time-resolved microwave conductivity (TRMC) measurements, although with no apparent impact of the phase transition.[28] We note that TRMC and OPTP spectroscopy probe charge-carrier mobilities with different time resolutions and range of charge-carrier motion.[57] TRMC probes over a longer time scale and is more impacted by the presence of excitons, trapping, and interface effects. We also note that previous experiments have probed charge transport by the spatial profile of emission, where resonance energy transfer may also play a role in exciton diffusion mechanisms.[60] The OPTP experiment, in contrast, probes short-range transport immediately after photoexcitation, and as we discuss later, reflects mainly free charge-carrier transport.[29] With OPTP, we are therefore able to, for the first time, reveal experimentally the impact of the changes in effective mass[60] at the phase transition of $(BA)_2PbI_4$.

### 2.3. Charge-Carrier Dynamics

To investigate the charge-carrier dynamics within the 2D perovskite films, we obtained the time-resolved OPTP photoconductivity signal by scanning the time delay between the optical pump and the THz probe pulses. We observed a very fast initial decay of the OPTP ΔS signal over the first few picoseconds upon 3.1 eV photoexcitation, significantly above the band gap, as shown in Figure 3b,d. To determine the nature of charge carriers that give rise to the OPTP signal, we acquired the frequency-resolved THz photoconductivity by scanning the time-domain profile of the THz probe and applying a Fourier transform. The real and imaginary parts of the photoconductivity spectra of PEPI and BAPI at room temperature and delay time of 2 ps after photoexcitation are shown in Figure 3c,e. We note the presence of phonon modulations superimposed with the spectra, which are associated with photoinduced shifts of the phonon resonances.[61–63] Aside from such phonon modulations, the photoconductivity spectra are in good agreement with the Drude model of conductivity arising from the acceleration of free charge carriers under the THz electric field and experiencing random scattering events.[57,64–66] The absence of a negative imaginary component in the complex photoconductivity spectra is contrary to previous observations in perovskite semiconductors presenting quantum confinement, or at temperatures below the exciton binding energy,[58,67,68] in which the frequency-resolved conductivity is known to deviate from

the traditional Drude formula.[66,69–71] The Drude-like spectra obtained for PEPI and BAPI agree with the evidence of band-like in-plane transport from the temperature-dependent mobilities, and indicate a negligible contribution of localised charge carriers or excitonic resonances to the OPTP signal (see simulated spectrum with excitonic resonances in Figure S9, Supporting Information). We note that previous reports of OPTP measurements in 2D perovskites have indicated stronger localization effects.[72] However, our experiments are performed over a limited range of low THz frequencies which are more sensitive to free charges. Furthermore, the orientation of the organic barriers may also affect the scattering rates if positioned perpendicular to the THz electric field which lies along the substrate plane. However, given that the semiconductor planes in our 2D perovskite films are highly oriented parallel to the film and substrate, our measurements reveal that the transport along such planes is actually intrinsically band-like. Based on these observations, we conclude that the photoconductivity transients displayed in Figure 3b,d is associated with a free charge-carrier population exhibiting Drude-like band transport.

Having established that the OPTP transients arise from free charge-carrier populations, we proceed by investigating the origins of the pronounced and rapid decay of photoconductivity observed at early times. To disentangle the multiple photophysical processes occurring over the first picoseconds after photoexcitation, we developed a new experiment for monitoring the photoconductivity and transient absorption (TA) in parallel, in situ, for a given sample. Our experiment measures the differential transmission ΔT/T of a broadband optical probe simultaneously to the acquisition of OPTP photoconductivity transients. **Figure 4**d,e shows the TA spectra of PEPI and BAPI . As the optical band-edge is dominated by the excitonic absorption in these materials, the exciton contribution also dominates the TA spectra at the band-edge. Although we observe little contribution from band-filling photobleach, we note that the presence of free charge carriers contributes to screening, and therefore reduces the oscillator strength of the exciton. Therefore, the photobleach of the exciton transition is induced by the presence of both excitons and free charge carriers.[73] Consequently, the TA spectral lineshape can be successfully fitted as a combination of bandgap renormalisation and changes to the position, broadening, and amplitude of the exciton absorption peak[74] (see Section S7, Supporting Information, for details).

Figure 4a,b shows the dynamics of the exciton photobleach (PB) for PEPI and BAPI films. The simultaneous OPTP photoconductivity dynamics obtained in situ are shown as boundaries to the shaded blue area for comparison. Interestingly, unlike the OPTP photoconductivity, the PB dynamics do not exhibit a fast initial decay. This suggests that the overall charge-carrier population (excitons and free charge carriers combined) remains mostly unchanged over these early times, as would be expected for high-quality materials for which recombination should be negligible on the picosecond time scale. This observation points to the formation of excitons as responsible for the fast decay of OPTP photoconductivity, rapidly quenching the population of free charges that give rise to the ΔS signal.

We further proceed by analysing features associated with the thermal relaxation of charge-carriers from an initially "hot" population with elevated temperature, to a "cool" population

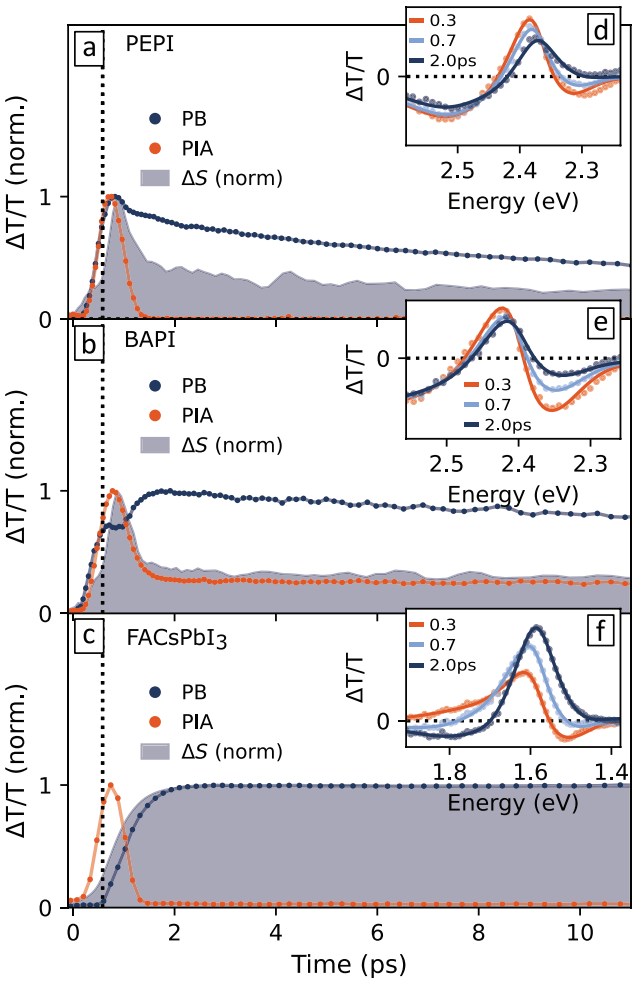


**Figure 4.** Transient absorption (TA) dynamics superimposed with the OPTP photoconductivity (ΔS) transients (boundaries to shaded area) acquired simultaneously in situ for a) PEPI , b) BAPI , and c) $FACsPbI_3$, at 295 K, 3.1 eV photoexcitation with 19 μJ $cm^{-2}$ fluence. The respective TA spectra are shown in d–f), where dots are experimental data and solid lines are fits to the model described in Section S1 (Supporting Information). The photobleach (PB) amplitude is taken from fits to the TA spectral lineshape and the subgap photoinduced absorption (PIA) is taken as the area of the negative signal below the band-edge.

reflecting the temperature of the surrounding lattice. Such charge-carrier cooling dynamics are often evaluated by fitting the high-energy side of the TA photobleach signal to a Boltzmann distribution.[74,75] However, this approach is not particularly valid in these 2D semiconductors, where exciton binding energies of hundreds of meV would result in a large separation between the excitonic photobleach and the edge of the continuum, and where we expect excitons to dominate the TA spectra at the optical band-edge. Alternatively, we analyse the subgap photoinduced absorption (PIA), because this has been demonstrated to correlate reasonably well with the cooling dynamics (see also Figure S13, Supporting Information).[75] We observe that charge-carrier cooling occurs over the first picosecond after photoexcitation and is convoluted with the experiment temporal resolution (Figures S21 and S22, Supporting Information). Interestingly, the fast initial decay of the OPTP

photoconductivity decay occurs over a similar timescale as the cooling dynamics. After thermal relaxation, the photoconductivity and TA photobleach follow the same dynamics (see Figure S19 (Supporting Information) over the following hundreds of picoseconds. These longer-time population dynamics present a distinctively bimolecular character evidenced by the fluence dependence of the transients (see Figure S16, Supporting Information). Similar fluence dependence is observed in the photoluminescence decays obtained by PL up-conversion transient spectroscopy (see Figure S18, Supporting Information). We therefore attribute the observed bimolecular dynamics to remaining free electron and hole populations encountering each other to recombine radiatively.

To help disentangle the effects of cooling, exciton formation, and population dynamics, we have also performed the combined OPTP and TA experiment using a film of 3D lead iodide perovskite $FACsPbI_3$, where FA is formamidinium (Figure 4c,f). The low $E_B \approx 10$ meV of $FACsPbI_3$, which is typical for these 3D metal halide perovskites,[67,76,77] leads to a negligible exciton population at room temperature.[29] This rise in photoconductivity concurrent with the charge-carrier cooling in $FACsPbI_3$ is in agreement with lower mobilities for hot charge carriers, resulting from the non-parabolicity of the band.[78,79] Following cooling, the photoconductivity and band-edge photobleach of $FACsPbI_3$ follow the same dynamics (see longer range in Figure S20, Supporting Information). The concurrent OPTP and TA dynamics and the absence of fast early decays in $FACsPbI_3$ support the assignment of the early OPTP dynamics of 2D perovskites to the rapid formation of excitons, quenching the population of free charge carriers while having minimal impact on the total charge-carrier population.

It is worth pointing out that the increase in charge-carrier mobilities observed during cooling in $FACsPbI_3$ may suggest that the mobilities in PEPI and BAPI (Figure 3a) measured at very early times may be slightly underestimated. However, we also note that the cooling dynamics in 2D Ruddlesden-Popper perovskites photoexcited at fluences below the hot-phonon bottleneck regime is expected to be faster compared to that of their 3D counterpart,[80–82] reducing such effects. Furthermore, in our experiments the energy offset between the 3.1 eV pump and the bandgap is lower in PEPI and BAPI than in the low-bandgap $FACsPbI_3$, which also contributes to faster cooling to the band-edge. Therefore, we conclude that, based on these observations, the early-time dynamics following photoexcitation of PEPI and BAPI are dominated by charge-carrier cooling and exciton formation, after which a quasi-equilibrium is established, and during which little charge-carrier recombination occurs. Our data show that such initial relaxation in PEPI and BAPI is essentially stabilized within the first 1–2 ps after 3.1 eV photoexcitation.

We further confirm these conclusions by performing the OPTP experiment also with pump-photon energy of 2.38 eV, that is, resonant with the exciton absorption peak of both PEPI and BAPI at room temperature. To facilitate comparison between the amplitudes for the two excitation energies (3.1 and 2.38 eV) and different temperatures, we show the signal in **Figure 5**a,b plotted as $\Delta\tilde{S}$, which equals $\Delta S$ normalised by the density of absorbed photons and by the charge-carrier mobility. For excitation with high-energy 3.1 eV photons significantly above the band edge, exciton formation results in a quick depletion of the initial free charge-carrier population, while the OPTP transients obtained with the 2.38 eV photoexcitation show no such fast initial decay. In addition,

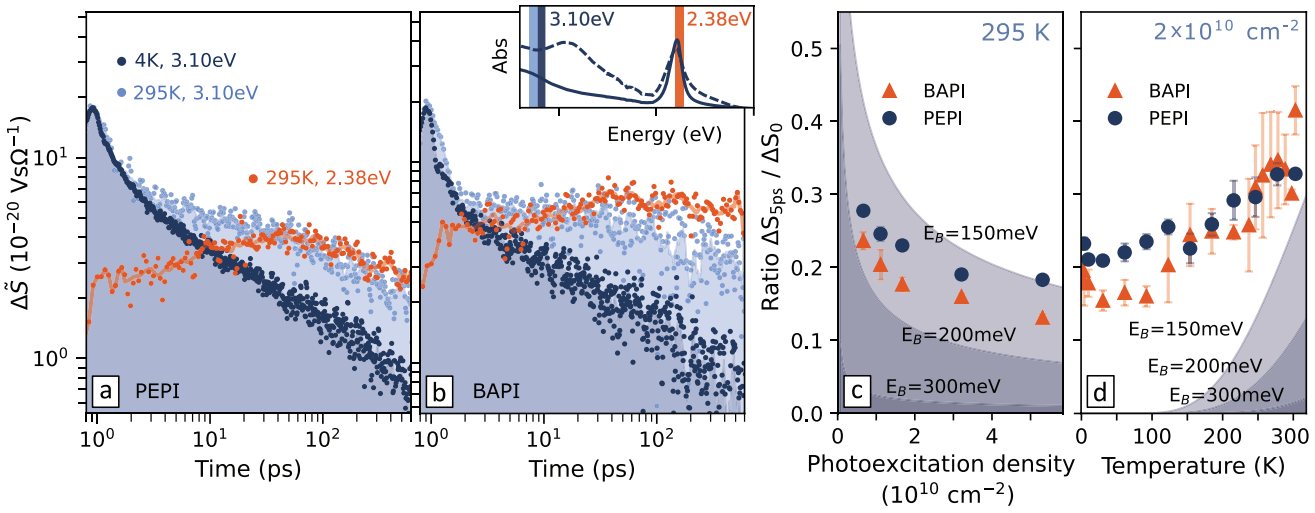


**Figure 5.** a,b) OPTP photoconductivity transients at comparable photoexcitation densities ($2.5\times10^{10}$ cm$^{-2}$) obtained at room temperature (295 K) with 3.1 eV excitation pulses (light blue) and 2.38 eV excitation (orange), and at 4K with 3.1 eV excitation (dark blue), for (a) PEPI and (b) BAPI. For better comparison, the signal is shown as $\Delta\tilde{S}$, which equals $\Delta S$ normalised by the area density of absorbed photons and by charge-carrier mobility (assuming the same mobility is experienced after 3.1 and 2.38 eV excitation but changes with temperature). For reference, the inset of (b) shows the normalised absorption spectra of PEPI (solid line) and BAPI (dashed line) with the excitation energies highlighted. c) Fraction of remaining free charge-carrier population taken from the ratio $\Delta S_{5ps}/\Delta S_0$ ratio, where $\Delta S_{5ps}$ is the OPTP signal taken at $t = 5$ ps, measured for PEPI and BAPI at room temperature and various photoexcitation densities, and d) at different temperatures, for constant photoexcitation density ($2 \times 10^{10}$ cm$^{-2}$). The photoexcitation densities per layer are calculated as a weighted average of absorbed photons per layer (see note in S9 for details).

regardless of the initial photoexcitation energy, the amplitude of the photoconductivity transients eventually reaches similar values for both above-gap and near-gap excitation. These observations also agree with photocurrent measurements, as we have recently reported,[29] which probe charge transport at longer ranges and timescales and therefore closer to equilibrium conditions. Given that the photoconductivity signal originates from free charge carriers, as previously discussed, the fast decay in the OPTP transients observed for above-gap 3.1 eV excitation thus derives from a higher, non-equilibrium fraction of free charge carriers initially generated, compared to excitation near the excitonic resonance, at 2.38 eV. However, once exciton formation has been completed within the first few picoseconds, we indeed observe that the populations of excitons and free charge carriers reach very similar quasi-equilibrium conditions, regardless of the excitation photon energy.

### 2.4. Exciton to Free Charge Carrier Ratios

Interestingly, the simultaneous TA and OPTP dynamics in Figure 4 shows that a significant photoconductivity signal is still present at quasi-equilibrium conditions, suggesting a substantial population of free charge carriers is preserved. This insight into exciton formation directs us to a key question in 2D perovskite photophysics[21]: what is the fraction of photogenerated free charge carriers that ultimately form excitons in equilibrium? The formalism most commonly employed to answer this question is the Saha equation,[83,84] which gives the equilibrium branching ratio $\alpha = n_{free}/n_0$, that is, the fraction of free-carrier density $n_{free}$ out of the total density of electron-hole pairs $n_0 = n_{free} + n_{ex}$ where $n_{ex}$ is the exciton density, according to

$$\frac{\alpha^2}{1-\alpha} = \frac{1}{n_0 (h/\sqrt{2\pi m^* k_B T})^d} \exp\left(\frac{-E_B}{k_B T}\right) \quad (1)$$

where $d$ is the semiconductor dimension, $T$ is the temperature, and $m^*$ is the electron-hole reduced mass. The shaded areas of Figure 5c,d shows the equilibrium fraction of free charge carriers $\alpha$ calculated by Equation 1 for different values of $E_B$ as a function of photoexcitation density and temperature in a sheet of 2D semiconductor.

We proceed by attempting to extract the equilibrium ratio $\alpha$ of the free-carrier density $n_{free}$ to the total density of electron-hole pairs from OPTP transients recorded for significant above-gap excitation (3.1 eV). We note that the main contrast between the Saha equation and conditions for our OPTP experiment is that the Saha equation represents an equilibrium situation. However, as we discussed above, a quasi-equilibrium condition can be considered to be reached after a few picoseconds following photoexcitation. Let us then assume that the amplitude of the OPTP signal at $t = 0$ arises from a population of free charge carriers, with no significant excitonic populations yet having been established. These charge carriers subsequently relax, with a fraction forming excitons and establishing an equilibrium between free charge carriers, by a given time after excitation, which we take here to have been completed by a reference point of 5 ps after excitation. Under the reasonable assumption that on this time scale, the charge-carrier mobility has not changed, and an insignificant fraction of charge carriers has recombined, the photoconductivity signal at $t = 0$ ($\Delta S_0$) can therefore be taken as reflecting the total density of electron-hole pairs in the system, before and after equilibrium has been reached, while the photoconductivity signal after the initial fast decay has occurred ($\Delta S_{5ps}$ taken at 5 ps) represents the density of free charge carriers $\alpha$ remaining at equilibrium. The value of $\Delta S_{5ps}$, divided by the signal $\Delta S_0$ at $t = 0$ therefore experimentally yields the ratio $\alpha$ of free charge-carrier density to total electron-hole pair density at equilibrium.

Figure 5c shows the fluence dependence of the extracted $\Delta S_{5ps}/\Delta S_0$ ratio measured for PEPI and BAPI films at room temperature. As predicted by the Saha equation, the fraction of remaining free-carrier photoconductivity after exciton formation decreases with increasing photoexcitation density, and is lower in BAPI compared to PEPI , in agreement with the higher $E_B$ in BAPI. The experimentally extracted values of $\alpha$ at room temperature are reasonably similar with the theoretical predictions, in agreement with our previous observations of long-range photocurrent measurements.[29] However, the decrease in $\Delta S_{5ps}/\Delta S_0$ ratio over increasing fluence is less pronounced than the theoretical prediction, suggesting free charge-carrier populations at room temperature may be higher than expected.

At low temperatures, the discrepancy between the $\Delta S_{5ps}/\Delta S_0$ ratio and the theoretical value of $\alpha$ predicted from the Saha equation is even more contrasting, as shown in Figure 5d. We find that at 4K, while the Saha equation predicts a value of $\alpha$ very close to zero, the experimentally determined value is closer to 0.2. In fact, the photoconductivity dynamics in Figure 5a,b indicates a significant population of free charge carriers that are not fully converted into excitons being preserved even after hundreds of picoseconds at 4K. Therefore, while the decrease in free charge-carrier populations with decreasing temperature qualitatively agrees with the expected thermally-activated exciton dissociation, this temperature dependence is far less severe than one would calculate from the Saha equation.

We point out that any instantaneous exciton formation or rapid dynamics[85] convoluted with the temporal resolution of the OPTP experiment may result in a slight underestimation of $\Delta S_0$, leading to somewhat elevated values for the free-charge fraction of the total charge-carrier pairs. However, only an underestimation factor as high as ≈30 would allow agreement of our observations with the Saha predictions within the experimental boundaries (see Section S10, Supporting Information). We note that any underestimation of $\Delta S_0$ would equally affect the photon-to-free-charge-branching ratio $\phi$, which we consider to be equal to 1 to derive the values of $\mu_{eff}$ plotted in Figure 3a. Any such severe inaccuracy by a factor of ≈30 would imply charge-carrier mobilities exceeding by an order of magnitude those typically recorded[58,67] for corresponding 3D lead iodide perovskites, which is highly unlikely. Therefore, we infer that our analysis is not significantly affected by any major underestimation of $\Delta S_0$.

We now discuss the possible origins of such surprisingly large populations of free charges in a quasi-equilibrium situation. We examine the two possible scenarios of suppression of initial exciton formation and generally enhanced exciton dissociation rates. The more pronounced deviations from the

Saha predictions at low temperatures suggest the presence of thermally-activated mechanisms. The stabilisation of separated electrons and holes in the form of large polarons may result in an energy barrier for the formation of excitons.[86] Another possible consideration is that free charge carriers immediately after photogeneration may fall into separate layers of the inorganic lattice. These polycrystalline n = 1 2D perovskites are formed by a regular layered structure, and the separation of electrons and holes by the organic spacer layers could hinder the formation of bound excitons. This rapid separation of charge carriers would be facilitated by the high charge-carrier mobilities, particularly at low temperatures, combined with the excess photoexcitation energy of the 3.1 eV pump. However, the OPTP transients do not indicate any significant variation in exciton-formation dynamics with temperature and excitation fluence, with similar timescales observed for the rapid early decay (see Figure S16, Supporting Information). Furthermore, as shown in Figure 5a,b, even direct photoexcitation of excitons results in similarly large free-charge populations at equilibrium, pointing to efficient dissociation mechanisms rather than suppressed exciton formation as the dominant factor driving such a remarkably high ratio of free charges.

The efficient dissociation of excitons in 2D perovskites has been previously reported to occur at interfaces and grain boundaries,[47,87] facilitated by fast exciton diffusion.[56] However, such effects are not expected to be as significant in the phase-pure $n = 1$ RP materials examined in the present work. Moreover, the high levels of crystallinity and homogeneity of the material is evidenced by long-range charge-carrier mobilities obtained by transient photocurrent methods recently reported.[29] We also highlight that no difference was observed when photoexciting from either side of the film (see Figure S23, Supporting Information). There are likely to be significant differences in the crystallinity, surface energy, and defect compositions across the various interfaces. The absence of any impact on the recorded transients therefore demonstrates a negligible impact of interfaces on the exciton dynamics and suggest that the observed efficient exciton dissociation rates are an intrinsic property of 2D RP perovskites.

Another factor to consider is the Coulombic screening of excitons by free charge carriers. However, significant screening is expected only above the Mott transition, estimated[88] to occur near charge-carrier densities of $2 \times 10^{11}$ cm$^{-2}$. We do not observe any increase in free charge population with increasing excitation fluence in our experiments. Hence we can safely assume our observations lie below the Mott transition.[72,88,89]

It is worth noting that while the Saha equation considers a unique exciton binding energy for the calculation of free-carrier population, both PEPI and BAPI present complex fine electronic structures indicating multiple contributions to the photogenerated populations. In fact, the complex exciton fine structures highlight the polaronic character of the excitons, which is an important aspect to consider.[36,39,86] The dynamic polaronic screening of the exciton has recently been proposed to reduce the effective binding energy, potentially enhancing exciton dissociation in 2D perovskites.[90,91] Intriguingly, our work presents two aspects that contrast with such previous reports. One is that such polaronic screening effects were suggested to be absent in strongly confined $n = 1$ 2D perovskites such as $(PEA)_2PbI_4$ and $(BA)_2PbI_4$, contrary to our observations of enhanced free-charge populations in these materials. Another interesting contrast is in our observation of large free-charge populations at low temperatures, which rule out a thermally-activated polaronic screening. We also propose that any heterogeneity in the energetic landscape present in these materials as a result of their lattice softness may promote the separation of charges. However, to preserve the agreement with the band-transport and high charge-carrier mobilities we report, any such effects must not result in strong charge localisation. Overall, our results point either towards the existence of significant polaronic screening even at 4K, or to further mechanisms stabilising a large population of free charge carriers, potentially through thermal fluctuations or local distortions.

Our investigation of photoconductivity and charge-carrier dynamics in PEPI and BAPI provides unequivocal evidence of deviations from the Saha equation which agree with previous observations for some low-dimensional perovskites.[28,86,90,91] Such deviations demonstrate how the commonly used theoretical treatments of 2D perovskite photophysics still fall short of an accurate description of the material behavior, and indicate that the relative free charge-carrier populations may be much higher than commonly expected. Although at this moment we are not able to determine which mechanism provides the dominant cause of these effects, we hope our findings will raise attention to this intriguing open question regarding the photophysics of 2D perovskites. Future insights and experimental strategies in this area may open possibilities to manipulate the exciton population for optimal device performance. Combined with the high charge-carrier mobilities and band transport (Figure 3a), our observations of large free charge-carrier populations demonstrate remarkably efficient in-plane charge transport properties in these layered semiconductors, despite strong dielectric confinement in the direction perpendicular to the organic spacer layers. We also highlight that the effects we report are particularly striking at low temperatures, for which we observe the most significant deviation from the expected relative exciton populations and the highest mobilities associated with band transport. This finding implies great potential for device applications optimised for low-temperature operation, such as in outer space.

## 3. Conclusion

In conclusion, we reveal optoelectronic and charge-transport properties for the 2D Ruddlesden-Popper perovskites $(PEA)_2PbI_4$ and $(BA)_2PbI_4$. We demonstrate high charge-carrier mobilities within the plane of the 2D semiconductor sheets, comparable to those encountered in the 3D counterparts, and band transport behavior reflected by increasing mobilities with decreasing temperature over the 4–295K range. We show that although $(PEA)_2PbI_4$ and $(BA)_2PbI_4$ exhibit similar levels of electronic confinement, bandgap energies, and emission properties at room temperature, the 2D perovskite with BA cations as a spacer is affected by enhanced coupling of charge-carriers to phonons, resulting in lower charge-carrier mobilities with respect to the case for PEA cations. Our OPTP measurements with high temporal resolution are exclusively sensitive to free

charge carriers, and, in combination with simultaneous TA acquisition, provide direct insight into the exciton formation process. Our observations reveal a large, long-lived relative population of free charge carriers that persists even at low temperatures, far exceeding the predictions of the Saha equation. The high fraction of free charge carriers, combined with remarkably high charge-carrier mobilities and band transport demonstrate exceptionally efficient charge transport properties in the plane of these layered semiconductors. Notably, the efficient charge-transport properties coexist with sharp emission from strongly-confined excitons that result from the low dimensionality of the material, providing an interesting and uncommon combination of functional characteristics. Our findings also demonstrate the potential of such materials for transistors and electrically driven light emitters. This efficient transport of free carriers is also a promising feature for their application in high-bandgap photovoltaics, provided that complete control over appropriate layer orientation is achieved in planar-architecture devices.

## 4. Experimental Section

*Sample Preparation*: Lead(II) iodide ($PbI_2$, 99.999%, metal basis) was purchased from TCI chemicals. Cesium iodide (CsI, 99.99%) was purchased from Alfa-Aesar. Formamidinium iodide (FAI) was purchased from GreatCell Solar. Phenylethylammonium iodide (PEAI), butylammonium iodide (BAI), dimethylformamide (DMF, anhydrous, 99.8%), dimethyl sulfoxide (DMSO, anhydrous, >99.9%), anisole (anhydrous, 99.7%), isopropyl alcohol (IPA), and acetone were purchased from Sigma–Aldrich. All chemicals were used as purchased without further purification unless stated otherwise.

*$FACsPbI_3$*: $PbI_2$, FAI, and CsI where mixed in a nitrogen-filled glovebox in ratios to yield the stoichiometry of $FA_{0.9}Cs_{0.1}PbI_3$. The precursors were then mixed with DMF:DMSO (3:1) to yield a 1.0 m precursor solution. After mixing for at least 3 h in the glovebox, 250 µL of solution was spin-coated dynamically onto clean glass or quartz substrates using a standardized program of 1000 rpm for 10 s then 5000 rpm (2000 rpm acceleration) for 35 s. The precursor solution was dropped at 5-6 s after the start of the program. Then, 350 µL of anisole was dropped onto the spinning film 35 s after the start of the program. It took 1-2 s to drop the anisole. Subsequently, the films were annealed at 100°C for 15 min.

*$(PEA)_2PbI_4$ and $(BA)_2PbI_4$*: Stoichiometric amounts of $PbI_2$ and PEAI/BAI were mixed in a nitrogen-filled glovebox with DMF to yield a 0.6 m precursor solution. After at least 3 h of mixing, the solution was spin- coated in a drybox using an optimized protocol: The film was spun at 1000 rpm for 10 s. After 5 s, 250 µL of precursor solution was dropped onto the spinning film. The spin speed was then increased to 6000 rpm (2000 rpm acceleration) for an additional 40 s. No antisolvent was needed. The films were annealed on a hotplate at 100°C for 15 min.

*Optical Characterisation*: Reflection and transmission spectra were measured using a Bruker 80v Fourier-transform infrared spectrometer with a tungsten halogen lamp source, a $CaF_2$ beamsplitter and a silicon diode detector. High temporal resolution time-resolved PL measurements were performed using upconversion PL spectroscopy. For these, the output of a tunable Ti:Sapphire oscillator (Spectra Physics Mai Tai, 80MHz, 100 fs pulse width) was split into a pump line and an optical gate. The samples were illuminated with 410 nm light obtained by frequency-doubling the 820 nm fundamental laser output. The PL collected from the sample was focused onto a BBO crystal, overlapped with the gate beam. The sum-frequency photons were then collected into a spectrometer and a CCD detector. The short pulse width of the optical gate determines the enhanced temporal resolution of the experiment. The time delay between the pump and the optical gate was varied using a linear translation stage for recording the PL dynamics.

*Optical-Pump THz-Probe (OPTP)*: Measurements were performed as previously described by Wehrenfennig et al.[92] The optical pump excitation was obtained by frequency doubling the fundamental laser output through a BBO crystal, resulting in 3.1 eV photons, or by tuning the output of an optical parametric amplifier to generate 2.38 eV photons. THz probe pulses were generated by a spintronic emitter which was composed of 1.8 nm of $Co_{40}Fe_{40}B_{20}$ sandwiched between 2 nm of tungsten and 2 nm of platinum, supported by a quartz substrate. Detection of the THz pulses was performed using electro-optic sampling in a (110)-ZnTe crystal (thickness 1 mm). The FWHMs of the beams for the pump and THz pulses at the sample were measured to be 2 mm and 0.5 mm respectively. The sample, THz emitter and THz detector were held under vacuum ($<10^{-2}$ mbar) during the measurements.

*Transient Absorption (TA)*: Measurements were performed simultaneously and in situ with the OPTP experiment. A broadband optical probe was generated by focusing a branch of the 800 nm fundamental output of the laser into a 3-mm c-cut sapphire disk. The optical probe was focused onto the sample (spot size FWHM of 150 µm) overlapped with the THz probe and optical pump, collected in transmission and detected with a silicon photodiode. The OPTP and TA dynamics were not affected by the presence of either probe beam. The time delay of the optical and THz probes were adjusted to be similar, but $t = 0$ was manually corrected for each. In addition, the wavelength dependence of $t = 0$ in the TA experiment was corrected according to the dispersion of the optical probe.

## Supporting Information

Supporting Information is available from the Wiley Online Library or from the author.

## Acknowledgements

The authors gratefully acknowledge support from the Engineering and Physical Sciences Research Council (EPSRC), Prosperity Partnership (EP/S004947/1). L.M.H. thanks TUM-IAS for a Hans Fischer Senior Fellowship and Award. MBJ thanks the EPSRC for the award of an Established Career Fellowship (EP/T025077/1). H.J.S. is cofounder and CSO of Oxford PV ltd, a company commercializing perovskite PV technology. The other authors declare no conflicts of interest.

## Conflict of Interest

The authors declare no conflict of interest.

## Data Availability Statement

The data that support the findings of this study are available from the corresponding author upon reasonable request.

## Keywords

excitons, perovskite semiconductors, photoconductivity, 2D perovskites

Received: January 10, 2023
Revised: March 20, 2023
Published online:

[1] NREL, Best Research-Cell Efficiencies, **2020**, https://www.nrel.gov/pv/cell-efficiency.html.
[2] M. V. Kovalenko, L. Protesescu, M. I. Bodnarchuk, *Science* **2017**, *358*, 745.
[3] N. Wang, L. Cheng, R. Ge, S. Zhang, Y. Miao, W. Zou, C. Yi, Y. Sun, Y. Cao, R. Yang, Y. Wei, Q. Guo, Y. Ke, M. Yu, Y. Jin, Y. Liu, Q. Ding, D. Di, L. Yang, G. Xing, H. Tian, C. Jin, F. Gao, R. H. Friend, J. Wang, W. Huang, *Nat. Photonics* **2016**, *10*, 699.
[4] M. Yuan, L. N. Quan, R. Comin, G. Walters, R. Sabatini, O. Voznyy, S. Hoogland, Y. Zhao, E. M. Beauregard, P. Kanjanaboos, Z. Lu, D. H. Kim, E. H. Sargent, *Nat. Nanotechnol.* **2016**, *11*, 872.
[5] K. Lin, J. Xing, L. N. Quan, F. P. G. de Arquer, X. Gong, J. Lu, L. Xie, W. Zhao, D. Zhang, C. Yan, W. Li, X. Liu, Y. Lu, J. Kirman, E. H. Sargent, Q. Xiong, Z. Wei, *Nature* **2018**, *562*, 245.
[6] K. Ji, M. Anaya, A. Abfalterer, S. D. Stranks, *Adv. Opt. Mater.* **2021**, *9*, 2002128.
[7] Y. Jia, R. A. Kerner, A. J. Grede, B. P. Rand, N. C. Giebink, *Nat. Photonics* **2017**, *11*, 784.
[8] S. Yakunin, L. Protesescu, F. Krieg, M. I. Bodnarchuk, G. Nedelcu, M. Humer, G. De Luca, M. Fiebig, W. Heiss, M. V. Kovalenko, *Nat. Commun.* **2015**, *6*, 8056.
[9] H. Zhu, Y. Fu, F. Meng, X. Wu, Z. Gong, Q. Ding, M. V. Gustafsson, M. T. Trinh, S. Jin, X.-Y. Zhu, *Nat. Mater.* **2015**, *14*, 636.
[10] C. Qin, A. S. D. Sandanayaka, C. Zhao, T. Matsushima, D. Zhang, T. Fujihara, C. Adachi, *Nature* **2020**, *585*, 53.
[11] L. Lei, Q. Dong, K. Gundogdu, F. So, L. Lei, Q. Dong, F. So, K. Gundogdu, *Adv. Funct. Mater.* **2021**, *31*, 2010144.
[12] Y.-S. Park, S. Guo, N. S. Makarov, V. I. Klimov, *ACS Nano* **2015**, *9*, 10386.
[13] H. Utzat, W. Sun, A. E. K. Kaplan, F. Krieg, M. Ginterseder, B. Spokoyny, N. D. Klein, K. E. Shulenberger, C. F. Perkinson, M. V. Kovalenko, M. G. Bawendi, *Science* **2019**, *363*, 1068.
[14] G. Rainò, M. A. Becker, M. I. Bodnarchuk, R. F. Mahrt, M. V. Kovalenko, T. Stöferle, *Nature* **2018**, *563*, 671.
[15] S.-W. Dai, B.-W. Hsu, C.-Y. Chen, C.-A. Lee, H.-Y. Liu, H.-F. Wang, Y.-C. Huang, T.-L. Wu, A. Manikandan, R.-M. Ho, C.-S. Tsao, C.-H. Cheng, Y.-L. Chueh, H.-W. Lin, *Adv. Mater.* **2018**, *30*, 1705532.
[16] F. Ricci, V. Marougail, O. Varnavski, Y. Wu, S. Padgaonkar, S. Irgen-Gioro, E. A. Weiss, T. Goodson, *ACS Nano* **2021**, *15*, 12955.
[17] L. Dou, A. B. Wong, Y. Yu, M. Lai, N. Kornienko, S. W. Eaton, A. Fu, C. G. Bischak, J. Ma, T. Ding, N. S. Ginsberg, L.-W. Wang, A. P. Alivisatos, P. Yang, *Science* **2015**, *349*, 1518.
[18] D. B. Mitzi, *J. Solid State Chem.* **1999**, *145*, 694.
[19] S. G. Motti, T. Crothers, R. Yang, Y. Cao, R. Li, M. B. Johnston, J. Wang, L. M. Herz, *Nano Lett.* **2019**, *19*, 3953.
[20] X. Li, J. M. Hoffman, M. G. Kanatzidis, *Chem. Rev.* **2021**, *121*, 2230.
[21] M. Righetto, D. Giovanni, S. S. Lim, T. C. Sum, *Appl. Phys. Rev.* **2021**, *8*, 011318.
[22] J.-C. Blancon, J. Even, C. C. Stoumpos, M. G. Kanatzidis, A. D. Mohite, *Nat. Nanotechnol.* **2020**, *15*, 969.
[23] I. C. Smith, E. T. Hoke, D. Solis-Ibarra, M. D. McGehee, H. I. Karunadasa, *Angew. Chem. Int. Ed.* **2014**, *53*, 11232.
[24] Z. Wang, Q. Lin, F. P. Chmiel, N. Sakai, L. M. Herz, H. J. Snaith, *Nat. Energy* **2017**, *2*, 17135.
[25] G. Grancini, C. Roldán-Carmona, I. Zimmermann, E. Mosconi, X. Lee, D. Martineau, S. Narbey, F. Oswald, F. De Angelis, M. Graetzel, M. K. Nazeeruddin, *Nat. Commun.* **2017**, *8*, 15684.
[26] S. Bellani, A. Bartolotta, A. Agresti, G. Calogero, G. Grancini, A. Di Carlo, E. Kymakis, F. Bonaccorso, *Chem. Soc. Rev.* **2021**, *50*, 11870.
[27] R. L. Milot, R. J. Sutton, G. E. Eperon, A. A. Haghighirad, J. Martinez Hardigree, L. Miranda, H. J. Snaith, M. B. Johnston, L. M. Herz, *Nano Lett.* **2016**, *16*, 7001.
[28] M. C. Gélvez-Rueda, E. M. Hutter, D. H. Cao, N. Renaud, C. C. Stoumpos, J. T. Hupp, T. J. Savenije, M. G. Kanatzidis, F. C. Grozema, *J. Phys. Chem. C* **2017**, *121*, 26566.
[29] M. Kober-Czerny, S. G. Motti, P. Holzhey, B. Wenger, J. Lim, L. M. Herz, H. J. Snaith, *Adv. Funct. Mater.* **2022**, 2203064.
[30] K. Tanaka, F. Sano, T. Takahashi, T. Kondo, R. Ito, K. Ema, *Solid State Commun.* **2002**, *122*, 249.
[31] K. Gauthron, J.-S. Lauret, L. Doyennette, G. Lanty, A. Al Choueiry, S. J. Zhang, A. Brehier, L. Largeau, O. Mauguin, J. Bloch, E. Deleporte, *Opt. Express* **2010**, *18*, 5912.
[32] D. B. Straus, S. Hurtado Parra, N. Iotov, J. Gebhardt, A. M. Rappe, J. E. Subotnik, J. M. Kikkawa, C. R. Kagan, *J. Am. Chem. Soc.* **2016**, *138*, 13798.
[33] D. B. Straus, C. R. Kagan, *J. Phys. Chem. Lett.* **2018**, *9*, 1434.
[34] F. Thouin, D. A. Valverde-Chávez, C. Quarti, D. Cortecchia, I. Bargigia, D. Beljonne, A. Petrozza, C. Silva, A. R. Srimath Kandada, *Nat. Mater.* **2019**, *18*, 349.
[35] A. R. Srimath Kandada, C. Silva, *J. Phys. Chem. Lett.* **2020**, *11*, 3173.
[36] F. Thouin, D. Cortecchia, A. Petrozza, A. R. Srimath Kandada, C. Silva, *Phys. Rev. Res.* **2019**, *1*, 032032.
[37] Y. Guo, O. Yaffe, T. D. Hull, J. S. Owen, D. R. Reichman, L. E. Brus, *Nat. Commun.* **2019**, *10*, 1175.
[38] W. Tao, Y. Zhang, H. Zhu, *Acc. Chem. Res.* **2022**, *55*, 345.
[39] L. Ni, U. Huynh, A. Cheminal, T. H. Thomas, R. Shivanna, T. F. Hinrichsen, S. Ahmad, A. Sadhanala, A. Rao, *ACS Nano* **2017**, *11*, 10834.
[40] M. C. Gélvez-Rueda, S. Peeters, P. C. Wang, K. M. Felter, F. C. Grozema, *Helv. Chim. Acta* **2020**, *103*, 2000121.
[41] M. Menahem, Z. Dai, S. Aharon, R. Sharma, M. Asher, Y. Diskin-Posner, R. Korobko, A. M. Rappe, O. Yaffe, *ACS Nano* **2021**, *15*, 10153.
[42] R. J. Elliott, *Phys. Rev.* **1957**, *108*, 1384.
[43] V. D'Innocenzo, G. Grancini, M. J. P. Alcocer, A. R. S. Kandada, S. D. Stranks, M. M. Lee, G. Lanzani, H. J. Snaith, A. Petrozza, *Nat. Commun.* **2014**, *5*, 3586.
[44] C. L. Davies, M. R. Filip, J. B. Patel, T. W. Crothers, C. Verdi, A. D. Wright, R. L. Milot, F. Giustino, M. B. Johnston, L. M. Herz, *Nat. Commun.* **2018**, *9*, 293.
[45] J.-C. Blancon, A. V. Stier, H. Tsai, W. Nie, C. C. Stoumpos, B. Traoré, L. Pedesseau, M. Kepenekian, F. Katsutani, G. T. Noe, J. Kono, S. Tretiak, S. A. Crooker, C. Katan, M. G. Kanatzidis, J. J. Crochet, J. Even, A. D. Mohite, *Nat. Commun.* **2018**, *9*, 2254.
[46] S. Neutzner, F. Thouin, D. Cortecchia, A. Petrozza, C. Silva, A. R. Srimath Kandada, *Phys. Rev. Mater.* **2018**, *2*, 064605.
[47] J.-C. Blancon, H. Tsai, W. Nie, C. C. Stoumpos, L. Pedesseau, C. Katan, M. Kepenekian, C. M. M. Soe, K. Appavoo, M. Y. Sfeir, S. Tretiak, P. M. Ajayan, M. G. Kanatzidis, J. Even, J. J. Crochet, A. D. Mohite, *Science* **2017**, *355*, 1288.
[48] J. Lee, E. S. Koteles, M. O. Vassell, *Phys. Rev. B* **1986**, *33*, 5512.
[49] C. Wehrenfennig, M. Liu, H. J. Snaith, M. B. Johnston, L. M. Herz, *J. Phys. Chem. Lett.* **2014**, *5*, 1300.
[50] A. D. Wright, C. Verdi, R. L. Milot, G. E. Eperon, M. A. Pérez-Osorio, H. J. Snaith, F. Giustino, M. B. Johnston, L. M. Herz, *Nat. Commun.* **2016**, *7*, 11755.
[51] R. H. Lyddane, R. G. Sachs, E. Teller, *Phys. Rev.* **1941**, *59*, 673.
[52] A. R. Srimath Kandada, H. Li, E. R. Bittner, C. Silva-Acuña, *J. Phys. Chem. C* **2022**, *126*, 5378.
[53] S. Poncé, M. Schlipf, F. Giustino, *ACS Energy Lett.* **2019**, *4*, 456.
[54] M. B. Johnston, L. M. Herz, *Acc. Chem. Res.* **2016**, *49*, 146.
[55] A. M. Ulatowski, L. M. Herz, M. B. Johnston, *J. Infrared Millim. Terahertz Waves* **2020**, *41*, 1431.
[56] M. Seitz, A. J. Magdaleno, N. Alcázar-Cano, M. Meléndez, T. J. Lubbers, S. W. Walraven, S. Pakdel, E. Prada, R. Delgado-Buscalioni, F. Prins, *Nat. Commun.* **2020**, *11*, 2035.
[57] L. M. Herz, *ACS Energy Letters* **2017**, *2*, 1539.
[58] R. L. Milot, G. E. Eperon, H. J. Snaith, M. B. Johnston, L. M. Herz, *Adv. Funct. Mater.* **2015**, *25*, 6218.
[59] L. R. V. Buizza, L. M. Herz, *Adv. Mater.* **2021**, *33*, 2007057.

[60] J. D. Ziegler, K.-Q. Lin, B. Meisinger, X. Zhu, M. Kober-Czerny, P. K. Nayak, C. Vona, T. Taniguchi, K. Watanabe, C. Draxl, H. J. Snaith, J. M. Lupton, D. A. Egger, A. Chernikov, *ACS Photonics* **2022**, *9*, 3609.
[61] D. Zhao, H. Hu, R. Haselsberger, R. A. Marcus, M.-E. Michel-Beyerle, Y. M. Lam, J.-X. Zhu, C. La-o vorakiat, M. C. Beard, E. E. M. Chia, *ACS Nano* **2019**, *13*, 8826.
[62] S. G. Motti, J. B. Patel, R. D. J. Oliver, H. J. Snaith, M. B. Johnston, L. M. Herz, *Nat. Commun.* **2021**, *12*, 6955.
[63] C. Q. Xia, S. Poncé, J. Peng, A. M. Ulatowski, J. B. Patel, A. D. Wright, R. L. Milot, H. Kraus, Q. Lin, L. M. Herz, F. Giustino, M. B. Johnston, *J. Phys.: Mater.* **2021**, *4*, 044017.
[64] J. Lloyd-Hughes, T.-I. Jeon, *J. Infrared, Millim. Terahertz Waves* **2012**, *33*, 871.
[65] M. C. Beard, G. M. Turner, C. A. Schmuttenmaer, *J. Phys. Chem. B* **2002**, *106*, 7146.
[66] M. C. Beard, G. M. Turner, C. A. Schmuttenmaer, *Nano Lett.* **2002**, *2*, 983.
[67] C. L. Davies, J. Borchert, C. Q. Xia, R. L. Milot, H. Kraus, M. B. Johnston, L. M. Herz, *J. Phys. Chem. Lett.* **2018**, *9*, 4502.
[68] S. G. Motti, F. Krieg, A. J. Ramadan, J. B. Patel, H. J. Snaith, M. V. Kovalenko, M. B. Johnston, L. M. Herz, *Adv. Funct. Mater.* **2020**, *30*, 1909904.
[69] N. Smith, *Physical Review B* **2001**, *64*, 155106.
[70] J. Lloyd-Hughes, H. E. Beere, D. A. Ritchie, M. B. Johnston, *Phys. Rev. B* **2008**, *77*, 125322.
[71] H. J. Joyce, J. L. Boland, C. L. Davies, S. A. Baig, M. B. Johnston, *Semicond. Sci. Technol.* **2016**, *31*, 103003.
[72] A. Burgos-Caminal, E. Socie, M. E. F. Bouduban, J.-E. Moser, *J. Phys. Chem. Lett.* **2020**, *11*, 7692.
[73] D. Huang, J.-I. Chyi, H. Morkoç, *Phys. Rev. B* **1990**, *42*, 5147.
[74] Y. Yang, D. P. Ostrowski, R. M. France, K. Zhu, J. van de Lagemaat, J. M. Luther, M. C. Beard, *Nat. Photonics* **2016**, *10*, 53.
[75] M. B. Price, J. Butkus, T. C. Jellicoe, A. Sadhanala, A. Briane, J. E. Halpert, K. Broch, J. M. Hodgkiss, R. H. Friend, F. Deschler, *Nat. Commun.* **2015**, *6*, 8420.
[76] L. M. Herz, *J. Phys. Chem. Lett.* **2018**, *9*, 6853.
[77] Y. Chen, S. G. Motti, R. D. Oliver, A. D. Wright, H. J. Snaith, M. B. Johnston, L. M. Herz, M. R. Filip, *J. Phys. Chem. Lett.* **2022**, *13*, 4184.
[78] M. C. Beard, G. M. Turner, C. A. Schmuttenmaer, *Phys. Rev. B* **2000**, *62*, 15764.
[79] M. Monti, K. D. G. I. Jayawardena, E. Butler-Caddle, R. M. I. Bandara, J. M. Woolley, M. Staniforth, S. R. P. Silva, J. Lloyd-Hughes, *Phys. Rev. B* **2020**, *102*, 245204.
[80] V. A. Hintermayr, L. Polavarapu, A. S. Urban, J. Feldmann, *ACS Nano* **2018**, *12*, 10151.
[81] C. Villamil Franco, G. Trippé-Allard, B. Mahler, C. Cornaggia, J. S. Lauret, T. Gustavsson, E. Cassette, *J. Phys. Chem. Lett.* **2022**, *13*, 393.
[82] J. Yin, P. Maity, R. Naphade, B. Cheng, J.-H. He, O. M. Bakr, J.-L. Brédas, O. F. Mohammed, *ACS Nano* **2019**, *13*, 12621.
[83] M. N. Saha, *Proc. R. Soc. London A* **1921**, *99*, 135.
[84] V. Sarritzu, N. Sestu, D. Marongiu, X. Chang, Q. Wang, M. A. Loi, F. Quochi, M. Saba, A. Mura, G. Bongiovanni, *Adv. Opt. Mater.* **2018**, *6*, 1700839.
[85] R. A. Kaindl, M. A. Carnahan, D. Hägele, R. Lövenich, D. S. Chemla, *Nature* **2003**, *423*, 734.
[86] A. Simbula, R. Pau, Q. Wang, F. Liu, V. Sarritzu, S. Lai, M. Lodde, F. Mattana, G. Mula, A. Geddo Lehmann, I. D. Spanopoulos, M. G. Kanatzidis, D. Marongiu, F. Quochi, M. Saba, A. Mura, G. Bongiovanni, *Adv. Opt. Mater.* **2021**, *9*, 2100295.
[87] E. D. Kinigstein, H. Tsai, W. Nie, J.-C. Blancon, K. G. Yager, K. Appavoo, J. Even, M. G. Kanatzidis, A. D. Mohite, M. Y. Sfeir, *ACS Mater. Lett.* **2020**, *2*, 1360.
[88] F. Thouin, S. Neutzner, D. Cortecchia, V. A. Dragomir, C. Soci, T. Salim, Y. M. Lam, R. Leonelli, A. Petrozza, A. R. S. Kandada, C. Silva, *Phys. Rev. Mater.* **2018**, *2*, 034001.
[89] A. Belogur, D. Baghdasaryan, I. Iorsh, I. Shelykh, V. Shahnazaryan, *Phys. Rev. Appl.* **2022**, *17*, 044048.
[90] W. Tao, Q. Zhou, H. Zhu, *Sci. Adv.* **2020**, *6*, 47eabb7132.
[91] Q. Sun, C. Zhao, Z. Yin, S. Wang, J. Leng, W. Tian, S. Jin, *J. Am. Chem. Soc.* **2021**, *143*, 19128.
[92] C. Wehrenfennig, G. E. Eperon, M. B. Johnston, H. J. Snaith, L. M. Herz, *Adv. Mater.* **2014**, *26*, 1584.